Cite This: J. Phys. Chem. A 2018, 122, 1270–1282

Heterogeneous Amyloid β -Sheet Polymorphs Identified on Hydrogen Bond Promoting Surfaces Using 2D SFG Spectroscopy

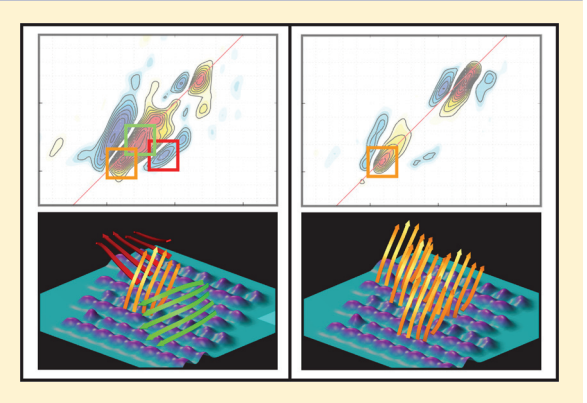
Published as part of The Journal of Physical Chemistry virtual special issue "Time-Resolved Vibrational Spectroscopy".

Jia-Jung Ho, Ayanjeet Ghosh, Tianqi O. Zhang, and Martin T. Zanni*

University of Wisconsin-Madison, Madison, Wisconsin 53706, United States

Supporting Information

ABSTRACT: Two-dimensional sum-frequency generation spectroscopy (2D SFG) is used to study the structures of the pentapeptide FGAIL on hydrogen bond promoting surfaces. FGAIL is the most amyloidogenic portion of the human islet amyloid polypeptide (hIAPP or amylin). In the presence of a pure gold surface, FGAIL does not form ordered structures. When the gold is coated with a self-assembled monolayer of mercaptobenzoic acid (MBA), 2D SFG spectra reveal features associated with β-sheets. Also observed are cross peaks between the FGAIL peptides and the carboxylic acid groups of the MBA monolayer, indicating that the peptides are in close contact with the surface headgroups. In the second set of samples, FGAIL peptides chemically ligated to the MBA monolayer also exhibited β-sheet features but with a much simpler spectrum. From simulations of the experiments, we



conclude that the hydrogen bond promoting surface catalyzes the formation of both parallel and antiparallel β -sheet structures with several different orientations. When ligated, parallel sheets with only a single orientation are the primary structure. Thus, this hydrogen bond promoting surface creates a heterogeneous distribution of polymorph structures, consistent with a concentration effect that allows nucleation of many different amyloid seeding structures. A single well-defined seed favors one polymorph over the others, showing that the concentrating influence of a membrane can be counterbalanced by factors that favor directed fiber growth. These experiments lay the foundation for the measurement and interpretation of β -sheet structures with heterodyne-detected 2D SFG spectroscopy. The results of this model system suggest that a heterogeneous distribution of polymorphs found in nature are an indication of nonselective amyloid aggregation whereas a narrow distribution of polymorph structures is consistent with a specific protein or lipid interaction that directs fiber growth.

INTRODUCTION

Molecular self-assembly is a fundamental strategy for the fabrication of nanoscale materials from small molecular building blocks¹⁻³ as well as a mechanism for toxicity in many amyloid diseases. 4-6 Self-assembled structures often form by nucleation and growth mechanisms⁷⁻¹⁰ that depend on the structures of nucleating seeds and the concentration of proteins that set free energy barrier heights. 11-13 Thus, surfaces that initiate nucleation via specific mechanisms or that simply increase the effective concentration of proteins could alter amyloid aggregate structures. 14 Indeed, nanostructures formed at interfaces can have different structures than in solution, forming alternative polymorphs. 15,16 Proteins involved in amyloid diseases, such as Alzheimer's and type-II diabetes, are well-known to be influenced by biological membranes like lipid bilayers as well as nonbiological surfaces like nanoparticles. 17-20 In vivo, there is evidence that amyloids involved in diseases have multiple polymorphs. 17,21

The 37-amino acid human islet amyloid polypeptide (hIAPP) aggregates into amyloid fibrils that are associated

with type-II diabetes. ^{22,23} These fibers contain β -sheet rich conformations. ^{24,25} Surfaces and interfaces are well documented to influence the aggregation of hIAPP. It is thought that the toxicity of hIAPP to cells is caused by polypeptides interacting with the cellular bilayer, perhaps by forming ion channels, or that the nucleation and growth process itself disrupts the membrane. ^{26,27} It has also been suggested that hIAPP interacts with specific membrane proteins and specific functionalized lipids, such as gangliosides. ²⁸

Most studies on hIAPP membrane interactions have focused on the amphipathic N-terminus region of hIAPP from residues 8–19, which most likely forms an α -helix on membrane bilayers. ^{29,30} It is less well understood how the segment from residues 20–29, or SNNFGAILSS, interacts with surfaces and membranes. This segment has been studied for many years because it is particularly crucial for amyloid fiber formation. ³¹

Received: December 4, 2017 Revised: January 4, 2018 Published: January 5, 2018



Rats and other species have mutations in this region that prevent the polypeptide from aggregating and eliminate its toxicity. Moreover, kinetics measurements have recently discovered an intermediate in which this region forms β -sheet. Thus, the NNFGAILSS appears to be the key to understanding both the aggregation mechanism and origin of the polypeptides toxicity.

Self-assembled monolayers (SAMs) of alkanethiols serve as model systems for probing surface effects such as hydrophobic, hydrophilic, and electrostatic interactions. The McCarley and coworkers found that the Alzheimer's disease related peptide $A\beta$ forms β -sheets on alkanethio SAMs. Thermore, the SAMs possibly play a seeding role in the aggregation. Theoretical investigations have also been done on $A\beta$ aggregation on alkanethiol SAMs comprising different headgroups using MD simulation, which indicate that electrostatic interactions between the peptide and the SAM headgroups play a vital role in the adsorption of peptide on monolayers.

Obtaining structural information about polypeptides on surfaces is experimentally challenging because standard structural biology techniques like high-resolution NMR and X-ray crystallography are difficult to apply at interfaces.³⁶ Vibrational spectroscopies are good techniques for studying membrane-bound protein structure because of the sensitivity of backbone amide-I vibrations to protein secondary structure.³⁷

Sum-frequency generation spectroscopy has been applied to a range of polypeptides on various surfaces, ^{38,39} including hIAPP on membrane monolayer. ⁴⁰ ATR-FTIR and IRRAS have also been used to study membrane-bound polypeptides. ^{41,42} These are all 1-dimensional spectroscopies. For studying protein structure in the bulk, two-dimensional infrared (2D IR) spectroscopy has become a very valuable tool. ^{43–46} 2D IR spectra contain a second frequency axis that correlates molecular vibrations through their couplings, creating cross peaks. 2D line shapes give information on environment and polarization conditions can be used to measure internal orientations. ⁴⁷ The increased spectral resolution of 2D spectroscopy is particularly useful for recognizing heterogeneous distributions of structures. ⁴⁸

Recently, a surface sensitive version of 2D IR spectroscopy has been developed that is called heterodyne-detected (HD) 2D SFG. 49–52 HD 2D SFG (hereafter called 2D SFG) replaces the probe pulse in a standard 2D IR spectrometer with heterodyne-detected SFG. Or, put another way, a pair of broad band femtosecond pulses (or a line-narrowed hole burning pump pulse) is added to a HD SFG experiment. Either way, the outcome is an SFG spectrum with a second frequency dimension, analogous to 2D IR spectroscopy. Thus, 2D SFG offers the best of both worlds: the interfacial structural information on SFG and the capability of 2D IR to extract coupling and dynamical parameters. There are other surface-specific 2D IR methods under development, but none that have yet been applied to proteins. S3

In this article, we report the structures formed by self-assembled FGAIL polypeptides in contact with carboxylic acid terminated monolayers using 2D SFG spectroscopy. Our data are consistent with the formation of at least four amyloid structures and orientations that includes both parallel and antiparallel β -sheets. If peptides are covalently linked to the SAMs, then a largely homogeneous distribution of β -sheets is generated. This approach gives new insights into structural ensembles of this important fragment of hIAPP and provides a new way of studying specific polymorphs at surfaces. Our

results suggest that heterogeneous distributions of amyloid structures are a signature of aggregation through nonspecific interactions in which a membrane catalyzes aggregation by increasing local concentrations, whereas a narrow distribution of polymorph structures is consistent with a well-defined aggregation pathway favored by a specific protein/membrane interaction.

MATERIALS AND METHODS

Peptide Synthesis. The FGAIL peptide was synthesized using standard FMOC chemistry. PAL–PEG–PS resin was employed to generate an amidated C-terminus to remove the extra charge of the carboxylate and better mimic the native hIAPP sequence. The N-terminus remains for chemical conjugation in later steps described below. Each amino acid was added with a double 2 h coupling. Peptide cleavage with 95% (v/v) TFA was followed by reverse phase HPLC to produce purified with electrospray ionization mass-spectroscopy and stored in HFIP at -20° C.

Preparation of Monolayers on Gold. Methyl 4mercaptobenzoate (MMB), obtained from Toronto Research Chemicals Inc., and 4-mercaptobenzoic acid (MBA), obtained from Sigma-Aldrich, were used without further purification. The MMB and MBA monolayers on gold were deposited using established protocols.⁵⁴ Fresh gold substrates (Platypus Technologies, 100 nm Au with 5 nm Ti adhesion layer on silicon $\langle 1,0,0 \rangle$ wafer, diced to ≈ 1 cm² area and rinsed with ethanol before use) were soaked in 1 mM MMB or MBA solutions in ethanol (Sigma-Aldrich, HPLC grade 99.9%) for 24 h. The substrates were then removed from solution, rinsed thoroughly with pure ethanol, and dried under a stream of nitrogen until the bulk water is removed. For the deposition of FGAIL, MMB- or MBA-coated gold substrates were prepared as described above, following which a 4 mM solution of FGAIL was added on the substrate and bulk water removed with nitrogen drying.

Chemical Conjugation of Peptide on MBA SAMs. The standard chemical conjugation process is applied between FGAIL peptide and the MBA monolayer. 55,56 Briefly, (1-ethyl-3-(dimethylamino)propyl)carbodiimide hydrochloride (EDC) and N-hydroxysuccinimide (NHS) were purchased from Sigma-Aldrich and used without further purification. The MBA monolayers were activated using a mixture of 0.2 M EDC and 0.05 M NHS for 2 h. Pretreatment of the monolayers surfaces with EDC and NHS to create amine-reactive ester groups is necessary to chemically ligate the primary amine of FGAIL peptides. For peptide conjugation, a 4 mM solution of FGAIL was added on the activated substrates, allowed to sit overnight. Following the conjugation, the substrates were rinsed thoroughly with Milli-Q water, which reduce the nonconjugated ester back to carboxylic acid so that the rest of monolayer is the same as without conjugation. The sample is dried under a stream of nitrogen after rinsing.

2D SFG Spectroscopy. The details of the 2D SFG spectrometer have been published before. The short, three-quarters of the output of a regeneratively amplified Ti:sapphire laser (800 nm, \approx 50 fs fwhm, \approx 4 mJ/pulse, 1 kHz) was used to pump an optical parametric amplifier (OPA). The signal and idler beams from the OPA were used for difference frequency generation in an AgGaS₂ crystal to generate \approx 25 μ J of mid-IR light. About 95% of the light was sent through the mid-IR pulse shaper using a transverse Ge acousto-optic modulator to create the pump pulse pair, and the remaining 5% was used as the

mid-IR probe pulse. The residual 800 nm light was frequency-narrowed using a 1 nm fwhm interference filter centered at 805 nm. The visible pulse and mid-IR pulses were focused using 30 and 20 cm lenses, respectively, and overlapped at the sample. For all the experiments reported here, the visible and all mid-IR pulses were p-polarized. A 735 nm short pass filter was used to remove undesired 800 nm light. The signal was dispersed using a monochromator and collected using CCD detector. To prevent sample degradation during the experiment, the sample was scanned in the xy-plane such that a spot on the sample was only probed for 5 min (i.e., 5000 laser shots). All spectra were collected at room temperature at waiting time $t_2 = 0$.

Theoretical Modeling of 2D SFG Spectra. The 2D SFG spectra are simulated using a vibrational exciton Hamiltonian, which has mostly been detailed in previous publications. 57,58 For the MBA monolayer calculations, we use the transition dipole coupling (TDC) model with local mode frequency equal to 1740 cm⁻¹. The transition dipole and the polarizability tensor of MBA were calculated by Gaussian 09.59 For the peptide calculation, the TDC model is used with the nearest neighboring coupling corrected by Jansen's (ϕ, ψ) angle map.⁶⁰ The local mode frequencies of the amide-I vibrations are also calculated using the nearest-neighbor frequency shift provided by Jansen's work. The coupling between MBA and the peptide is modeled by TDC. Diagonal disorder is set to 10 cm⁻¹ for the MBA monolayer and 20 cm⁻¹ for the peptide. All of the calculations have 5 cm⁻¹ off-diagonal disorder and an additional 10 cm⁻¹ homogeneous line width convoluted with the stick spectra. The Matlab-based simulation code, COSMOSS, is freely available on GitHub.61 COSMOSS can be used to simulate IR, SFG, 2D IR, and 2D SFG spectra for a given protein structure.

EXPERIMENTS AND SPECTRAL ASSIGNMENTS

2D SFG of MBA Monolayer. In general, a 2D SFG spectrum contains pairs of out-of-phase peaks, one on the diagonal created by transitions that include the fundamental ($\nu = 0 \rightarrow 1$) and a second from the overtone ($\nu = 1 \rightarrow 2$) transitions shifted off of the diagonal by the vibrational anharmonicity. In Figure 1, green boxes enclose diagonal peak pairs that have $\omega_{\text{pump}} = 1725$ and 1615 cm^{-1} . Also shown are purple boxes that enclose two sets of cross peaks, which also

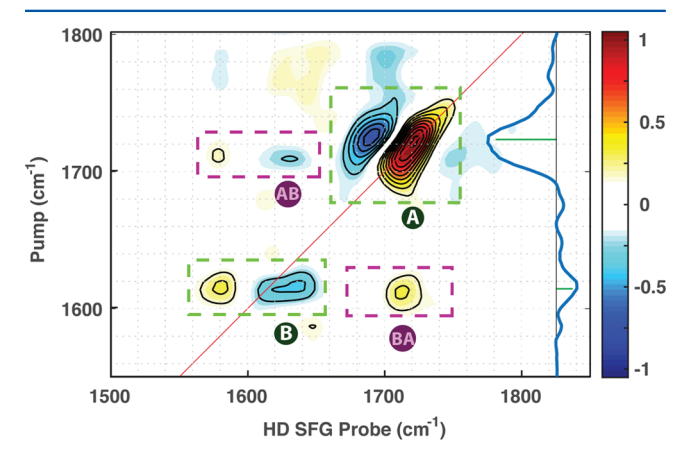


Figure 1. 2D SFG and the 2D diagonal cut (along the red line) of the 4-mercaptobenzoic acid (MBA) monolayer. The 2D spectrum is normalized to the most intense peak and plotted from -1 to +1 with contour steps of 10%, omitting the zero-level contour line.

appear as out-of-phase pairs. We labeled each box by its fundamental transitions, with A and B for the diagonal peaks pairs and AB and BA for the cross peaks. The cross peaks correlate the fundamental diagonal transitions A and B, giving cross peaks AB and BA. Only one cross peak is observed in box BA, because the overtone transition of that particular cross peak is comparable to the noise level. We only consider features with intensity above 10% of the maximum peak. The diagonal cut of the 2D SFG spectrum is shown as the blue line in Figure 1. The diagonal cut gives similar information as a more standard 1-dimensional heterodyne-detected SFG spectrum albeit with different peak intensities and line widths. We use this notation of single (A, B) and double (AB, BA) letters to signify diagonal and cross peaks throughout this article.

MBA (Figure 4a) has an aromatic ring with thiol and carboxylic acid functional groups at para positions to one another. On gold, the thiol groups bind weakly to the gold surface, creating tightly packed and well oriented monolayers with the carboxylic acid group exposed to air. Under the conditions used to make the films, the acid is protonated. Thus, peak A at 1725 cm⁻¹ comes from the carboxylic acid stretching mode. The vibrational frequency of carboxylic acid is usually set by the number of its hydrogen bonds: the antisymmetric stretching mode vibrates at ≈1740 cm⁻¹ without a hydrogen bond, $\approx 1720 \text{ cm}^{-1}$ when singly hydrogen-bonded, and ≈ 1700 cm⁻¹ when doubly hydrogen-bonded.⁶² The vibrational frequency is also affected by the local electrostatic environment as well as coupling to neighboring molecules. To characterize the origin of the frequency, we prepared a methyl 4mercaptobenzoate (MMB) monolayer on gold. MMB has a single hydrogen bond accepting site because the headgroup is an ester instead of a carboxylic acid. The ester group of MMB is measured at 1750 cm⁻¹ (Supporting Information), which is closer to the expected frequency of 1740 cm⁻¹ for no hydrogen bonding, indicating that the couplings and the electrostatic environment contribute $\approx 10 \text{ cm}^{-1}$ to the frequency. With this shift in mind, we assigned the vibrational frequency of peak A in MBA monolayer at 1725 cm⁻¹ to the singly hydrogen-bonded carboxylic acid stretching. The hydrogen bond may come from the neighboring carboxylic acid groups of MBA molecules or a thin hydration layer on top of the hydrophilic surface that is expected to remain after drying. The diagonal line width of peak A is about 40 cm⁻¹ and the antidiagonal line width is about 20 cm⁻¹, which indicates about 20 cm⁻¹ inhomogeneous broadening. This 20 cm⁻¹ inhomogeneity is about the same frequency difference between the different hydrogen bonding states of the carboxylic acid group, and so both the doubly hydrogen-bonded and non-hydrogen-bonded states might also contribute to the spectrum in lesser amounts.

Peak B at 1615 cm^{-1} originates from the benzoic ring stretching of MBA, close to the typical benzoic ring stretching frequency at $\approx 1600 \text{ cm}^{-1}$ in the gas phase.⁶³ The line width of the ring mode is about 10 cm^{-1} in both diagonal and antidiagonal directions, which suggests a well-ordered monolayer with uniform benzoic ring orientation.

Peak A has a larger 2D SFG intensity than peak B, which is consistent with the carboxylic acid mode having a stronger transition-dipole (μ) but weaker Raman-tensor (α) than the benzoic ring mode. Because a 2D SFG signal is proportional to $(\alpha \times \mu^3)$, peak A is expected to be larger than peak B. Furthermore, peak A is positive and peak B is negative. The sign of a heterodyne experiment tells us the direction of a mode projected onto the laser polarizations. In this experiment, all

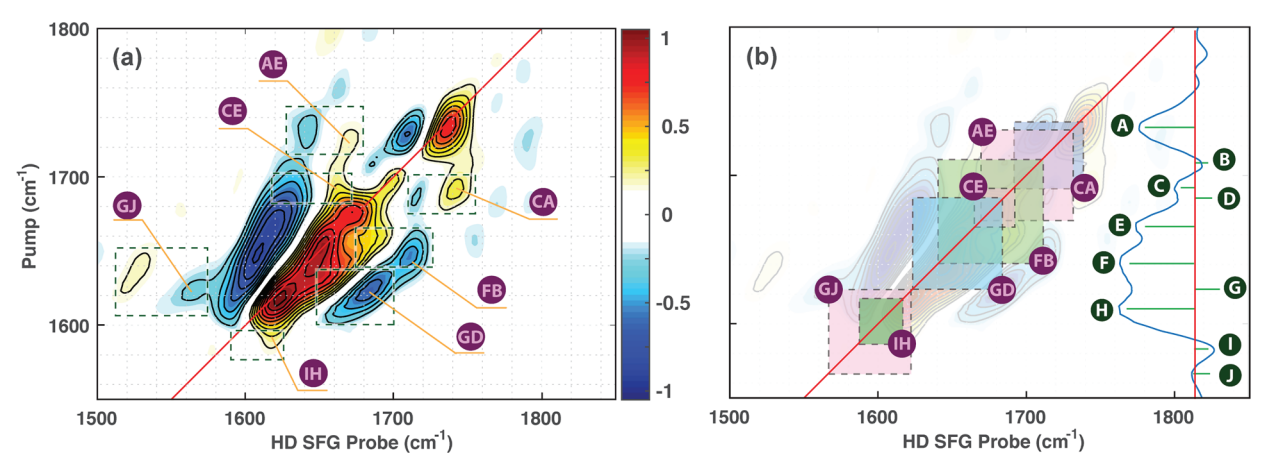


Figure 2. (a) 2D SFG of FGAIL aggregated on an MBA monolayer. Both the fundamental and overtone pathways of a cross peak are enclosed by a dashed box with a corresponding label pointing to the fundamental pathway. (b) Map showing the association between diagonal and cross peaks giving rise to the assignments shown with the diagonal cut through the 2D SFG spectrum (the blue curve). Green labels are diagonal peaks; purple labels are cross peaks. For clarity, the map only shows the labels on the fundamental pathways of the corresponding cross peaks. The diagonal vertices of a square box locate the coupled eigenstates that generate the corresponding cross peak(s) on the off-diagonal vertices on the same box.

laser beams are p-polarized, so the sign difference between A and B indicates that they have opposite transition-dipole directions. ^{57,65}

2D SFG of FGAIL Peptide on MBA Monolayer. Figure 2 is the 2D SFG spectrum of the FGAIL peptide aggregated on an MBA monolayer, which we refer to as FGAIL-MBA. The spectrum contains features from FGAIL and MBA, and as we show below, there are multiple FGAIL structures. Not available from standard SFG spectroscopy, the cross peaks help resolve spectra congestion from overlapping features of multiple structures.

In Figure 2a, we identify the fundamental and overtone pair of cross peaks as enclosed in green dashed boxes. We draw square boxes on top of the 2D SFG spectrum in Figure 2b by using the identified fundamental pathway of cross peaks as one of their vertices. The diagonal vertices of each square box are aligned with the red diagonal line of the 2D SFG spectrum. The diagonal vertices of a box in Figure 2b locate the coupled vibrational eigenstates that give the corresponding cross peak(s) on either one or both sides of the off-diagonal vertices. Take the cross peak CA, for example; we drew the blue box in Figure 2b and identified the coupled eigenstates A and C, which we labeled on the diagonal cut of the 2D SFG spectrum to the right-hand side of Figure 2b.

By using the vertical-aligned sign rule, ⁵⁷ which states that the diagonal and cross-peak with the same probe frequency have the same sign, we identify the sign for each of the diagonal peaks. For example, cross peak FB is negative, which means that its corresponding diagonal peak, vertically displaced (i.e., peak B), is also negative, even though it is not well resolved in the diagonal cut of the 2D SFG spectrum. In a heterodyne-detected 2D SFG, the opposite signs between peaks such as F and B are expected due to different orientations. ⁶⁵ Being able to assign unresolvable eigenstates with correct peak signs is crucial for extracting molecule orientation, coupling strength, and other information by matching spectral simulations.

Using this method, we systematically identified ten vibrational modes (A to J) and labeled them on the diagonal cut of the 2D spectrum to the right-hand side of Figure 2b. On the basis of the vibrational frequency of the monolayer, we know that peak A and B come from the carboxylic acid stretching and the peaks I and J originate from the benzoic ring stretching. We

assign peaks C to H as β -sheet modes. The peaks G and H near $1620~{\rm cm}^{-1}$ are the well-known collective vibrations across β -sheet strands. Likewise, peaks between $1660~{\rm and}~1680~{\rm cm}^{-1}$ are well-known modes for antiparallel β -sheets. Thus, visual inspection of the protein peaks in this spectrum informs us that the FGAIL polypeptide forms antiparallel sheets on the MBA surface, and the lower energy features are consistent with parallel sheets as well, which we confirm below in our simulations.

Also present are cross peaks between the FGAIL peptides and the MBA headgroups. The cross peaks AE at (1670, 1730) cm⁻¹ and CA at (1740, 1690) cm⁻¹ come from coupling between the carboxylic acid group of MBA (peak A) and the high-frequency vibrations of the antiparallel β -sheets. Thus, the coupling between the FGAIL peptide and MBA must be very strong to create these cross peaks, presumably due to a structural conformation in close contact with the self-assembled monolayer. Indeed, the MBA portion of the spectrum (peaks A, B) is different when FGAIL is applied. Comparing the pure MBA monolayer spectra in Figure 1 with FGAIL-MBA in Figure 2, we see that the carboxylic acid stretching blue (peak A) is shifted by 5 cm⁻¹ to 1730 cm⁻¹ and has a narrower diagonal line width. Likewise, the I and J modes are red-shifted by ≈ 35 cm⁻¹ from the benzoic ring stretching of a pure MBA monolayer in Figure 1. Because nothing else is different between sample preparations except the addition of the peptides, both the frequency shift and the line width change are attributed to peptides that couple or alter the MBA. Thus, the cross peaks, vibrational frequencies, and line widths are all indicators of strong interactions between the peptides and monolayer.

The vibrational frequency from the peptide peak F at ≈ 1650 cm⁻¹ could stem from three kinds of vibrations: the amide-I vibration of a random coil, the collective amide-I vibrations along the helical axis of an α -helix, or an eigenstate of a small β -sheet. Of these, only the small β -sheet is fully consistent with the data, for two reasons. First, by symmetry, the random coil is invisible in 1D SFG so it would not be able to generate a 2D SFG diagonal peak. Second, there are only four peptide bonds in an FGAIL sequence, which is insufficient to form a stable α -helix. Moreover, an α -helix cannot satisfy both the diagonal (F) and cross peak (FB) intensities in Figure 2 because the FB

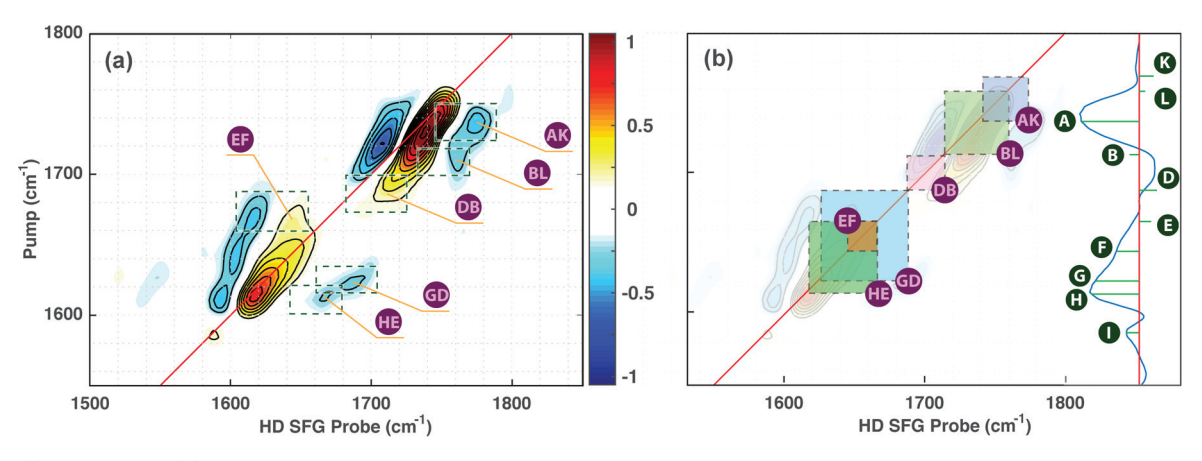


Figure 3. (a) 2D SFG and (b) peaks association map with diagonal cut of FGAIL tethered on MBA monolayer. Similar to Figure 2, the purple labels indicate the cross peaks, which are enclosed by dashed boxes in (a) and the green labels in (b) are diagonal peaks.

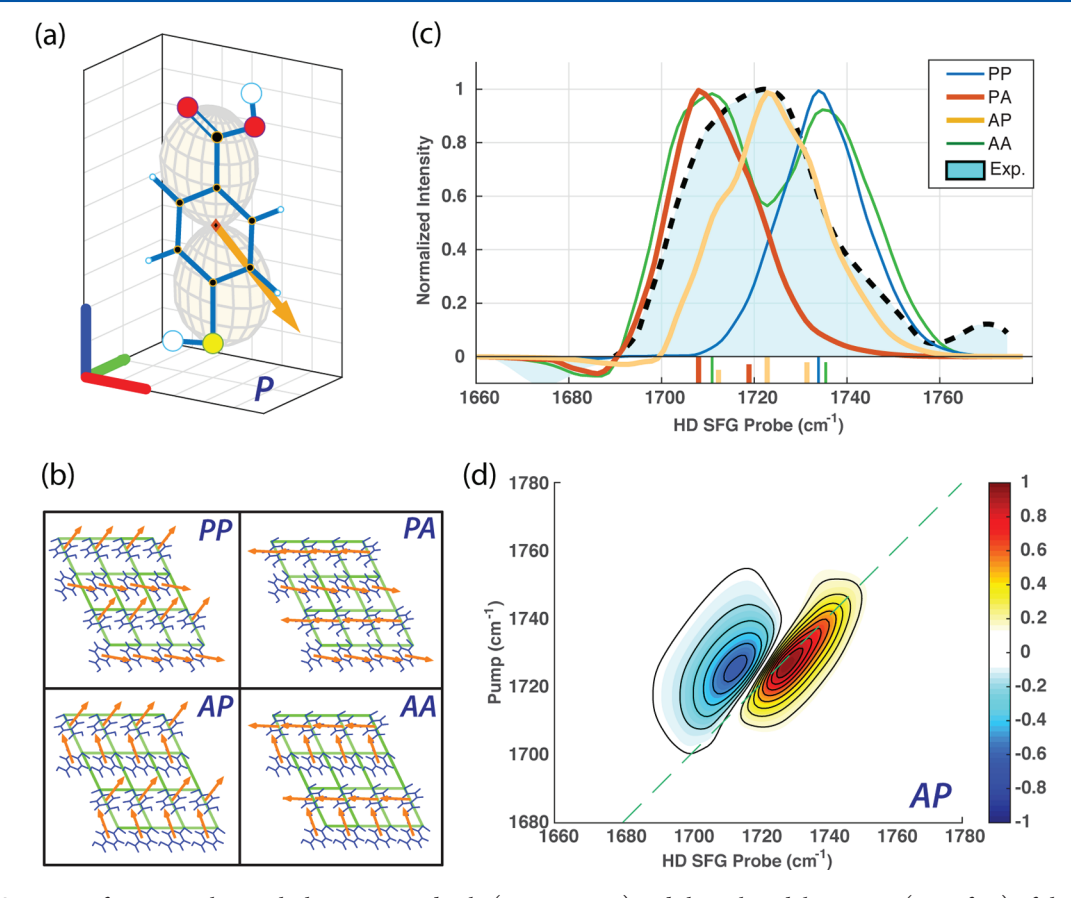


Figure 4. (a) Structure of MBA overlays with the transition dipole (orange arrow) and the polarizability tensor (isosurface) of the carboxylic acid stretching. (b) Top-down view of the model 2D lattices of the MBA monolayer. The orange vectors are the transition dipoles, and the green line outlines the unit cell lattice. (c) Diagonal cuts of the simulated 2D SFG spectrum of the MBA monolayers on top of the experimental diagonal cut. The sticks shown on the probe frequency axis represent the eigenstates of the corresponding diagonal cut. (d) Simulated 2D SFG spectrum of MBA lattice PA.

cross peaks requires a horizontal α -helix but that orientation would have little to no absorption, and thus a very weak diagonal peak. The remaining option is a β -sheet transition, which we show is consistent to the data, in later sections.

2D SFG of FGAIL Peptide Tethered on an MBA Monolayer. To test our hypothesis of polymorphism in a later section and limit possible peptide orientations, we chemically cross-linked the MBA monolayer with the FGAIL peptide. The detailed procedure of cross-linking is described in the Materials and Methods section. As expected, the 2D SFG spectrum of the

covalently linked FGAIL sample (Figure 3) is much simpler than the nonlinked sample (Figure 2). When we apply the same peak assignment procedure as above, we again found 10 eigenstates in Figure 3, but the FGAIL modes between 1660 and 1690 cm $^{-1}$ are much weaker. All the eigenstates are labeled on the diagonal cut of the 2D SFG spectrum in the right-hand side of Figure 3b. For eigenstates having similar frequencies within $\pm 5~\text{cm}^{-1}$ from those in the FGAIL-MBA sample, we simply assign them as the same vibrations with the corresponding labels used in Figure 2. Besides peaks C and J,

all eigenstates in Figure 2 show up in Figure 3. Thus, we conclude that the antiparallel β -sheet structures that make the 1660-1670 cm⁻¹ modes are now much less populated on the tethered FGAIL-MBA surface. The only new peaks are near 1760 cm⁻¹, which are from the imide bond that is created by the cross-link between peptide and headgroups. That assignment is consistent with DFT calculations (Supporting Information), which predicts a frequency of $\approx 1760 \text{ cm}^{-1}$, as well as a smaller transition dipole and the Raman tensor for the imide than the amide groups, which is why the cross peak AK and BL are apparent, but the diagonal peaks are weak. Although we cannot quantify the cross-linking yield, the fact that we can clearly see the carboxylic acid stretching mode at peak A indicates that not all of the headgroups are cross-linked. Except for the cross-linked residues, there are no cross peaks between the FGAIL peptide and the MBA headgroups. This is in contrast to FGAIL in Figure 2, where large cross peaks were observed. Thus, the 2D SFG spectra must contain similar β sheet structures and orientations because the same 10 peaks are present, but there is now a much lower population of antiparallel β -sheets.

SIMULATIONS AND DISCUSSION

To simulate the experimental spectra, we use an exciton description that relates the vibrational frequencies and couplings to the molecular structure. The model has been described in detail previously, and the simulations code has been made available through our Web site. The code can also be used to calculate IR, SFG, and 2D IR as well as 2D SFG spectra.

In the sections that follow, we first simulate the portion of the spectrum corresponding to the MBA monolayer. We then present simulations of the FGAIL peptide in various β -sheet structure and orientations and create an ensemble that explains the experiments. We conclude with a discussion on the influences of the hydrogen bonding interactions on the structure of the FGAIL aggregates.

MBA Monolayer. The structure of an MBA monolayer has been studied previously both experimentally and theoretically. X-ray photoelectron spectroscopy (XPS) and scanning tunneling microscopy (STM) were used to obtain lattice constants and DFT calculations provided an approximate molecular orientation. The monolayer forms a $\sqrt{3} \times 4$ unit cell with two MBA molecules. In the unit cell, the molecular axes are tilted by 37.4° (bridge-hcp) and 33° (bridge-fcc) from the surface normal. We use these structural parameters to build a 4-by-4 MBA monolayer model (Figure 4b). To simulate the spectrum of this model, we assigned each carboxylic acid a transition dipole (Figure 4a) and other factors, as described in the Supporting Information.

One unknown consideration with the MBA monolayer is the location of the hydrogen on each carboxylic acid. Due to the resonance structure stabilization between the benzene ring and the C=O double bond, the carbonyl group will be either parallel (P) or antiparallel (A) to the thiol group. The previous work on MBA monolayers could not resolve the hydrogen that dictates the geometry orientation. In our experiments, the coupling between adjacent MBA molecules spans a range from $\approx 6 \text{ cm}^{-1}$ for carboxylic acid headgroups pointed in the same direction (side-by-side) to $\approx -8 \text{ cm}^{-1}$ if pointed head to tail. Thus, the 2D SFG spectrum would be expected to change significantly depending on headgroup packing. With the 4-by-4

model that adopts one carbonyl group orientation in each row, we model four possibilities, which we labeled as PP, PA, AP, and AA, in Figure 4b.

Shown in Figure 4c are the diagonal slices through the 2D SFG spectrum of the MBA monolayers plotted for each of the four monolayer geometries in Figure 4b. Each structure of monolayer has a different frequency and line shape. Of these four scenarios, the best match to experiment is AP, which we use as the default packing arrangement in the rest of the simulations below. However, all of these structures are predicted to fall within the experimental 2D SFG line width. Thus, they may each contribution, albeit with different populations. A more thorough exploration might simulate a larger range of permutations as well as use isotope labeling to better interrogate the couplings. It is also interesting to note that linear SFG spectroscopy would not be as sensitive to these differences because of worse spectral resolution. Regardless, for the purposes of this manuscript, the results in Figure 4 are sufficient, because the focus is on the structure of the FGAIL aggregate.

Simulations of FGAIL Peptide. Efficient Calculation Procedure. In general, a system containing N vibrational local modes has $O(N^4)$ Feynman excitation pathways. As a result, calculating 2D SFG spectra for a protein structure is computationally expensive. Fitting or simulating experimental data to determine a structure and its orientation is even more computationally demanding because of the number of variables that must be optimized. Each peak in the 2D SFG spectrum has an intensity and sign that depends upon the transition dipole vectors and polarizability tensors, as well as the angles of the incident pulses and polarizations for the (up to four) eigenstates involved in each excitation pathway. Although they are not all resolved, a 2D SFG spectrum will contain dozens of overlapping peaks for a small polypeptide. In the past, we calculated 2D SFG spectra for each possible structure and its orientations and compared them to the experimental spectra.⁵⁷ Though that procedure is simple, it is a very timeconsuming process, mostly because the molecular response is calculated for each orientation. In the study here, we rewrite the response function, so that the molecular response, $\vec{\beta}^{(4)}$, only needs to be calculated once. The molecular response is then multiplied by the orientation tensor, \hat{R} , to get the orientation dependency of the signal. Of all the steps, the molecular response is the most time-intensive calculation. The cost savings of calculating the molecular response allows a more thorough investigation of the orientations and structures. The formalism for this approach is as follows, starting with the most standard equation for the describing the 2D SFG signal, S. 65,67

$$S(\phi, \psi, \theta) = N_{s} \cdot E \cdot J \cdot L \cdot \langle R \rangle \cdot \vec{\beta}^{(4)}(\phi, \psi, \theta)$$
 (1)

where $\vec{\beta}^{(4)}(\phi,\psi,\theta)$ is the fourth-order molecular response at a given molecular orientation noted by the Euler angles, R transforms the molecular response from molecule frame (x, y, z) to the lab frame (X, Y, Z), L is the local field correction factor, J converts the lab frame response from Cartesian coordinate (X, Y, Z) to the Jones coordinate (p, s), E describes the polarization states (p, s) and the intensity of the laser pulses, and N_s is the surface number density of the molecule. The brackets $\langle \cdots \rangle$ around R represent the ensemble average over the orientational distribution of the molecules on the surface.

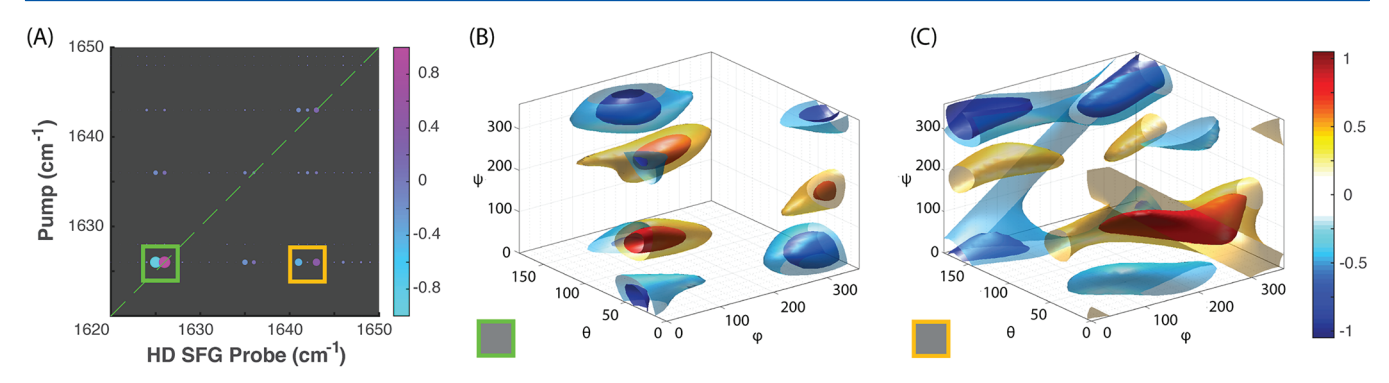


Figure 5. (A) Transition strength spectrum of the three strands canonical β-sheet shown in Figure 6A-3. (B), (C) Normalized 2D SFG signal orientation dependency maps calculated by eq 1. The colored boxes give a visual guidance between the regions of interest and their orientation maps.

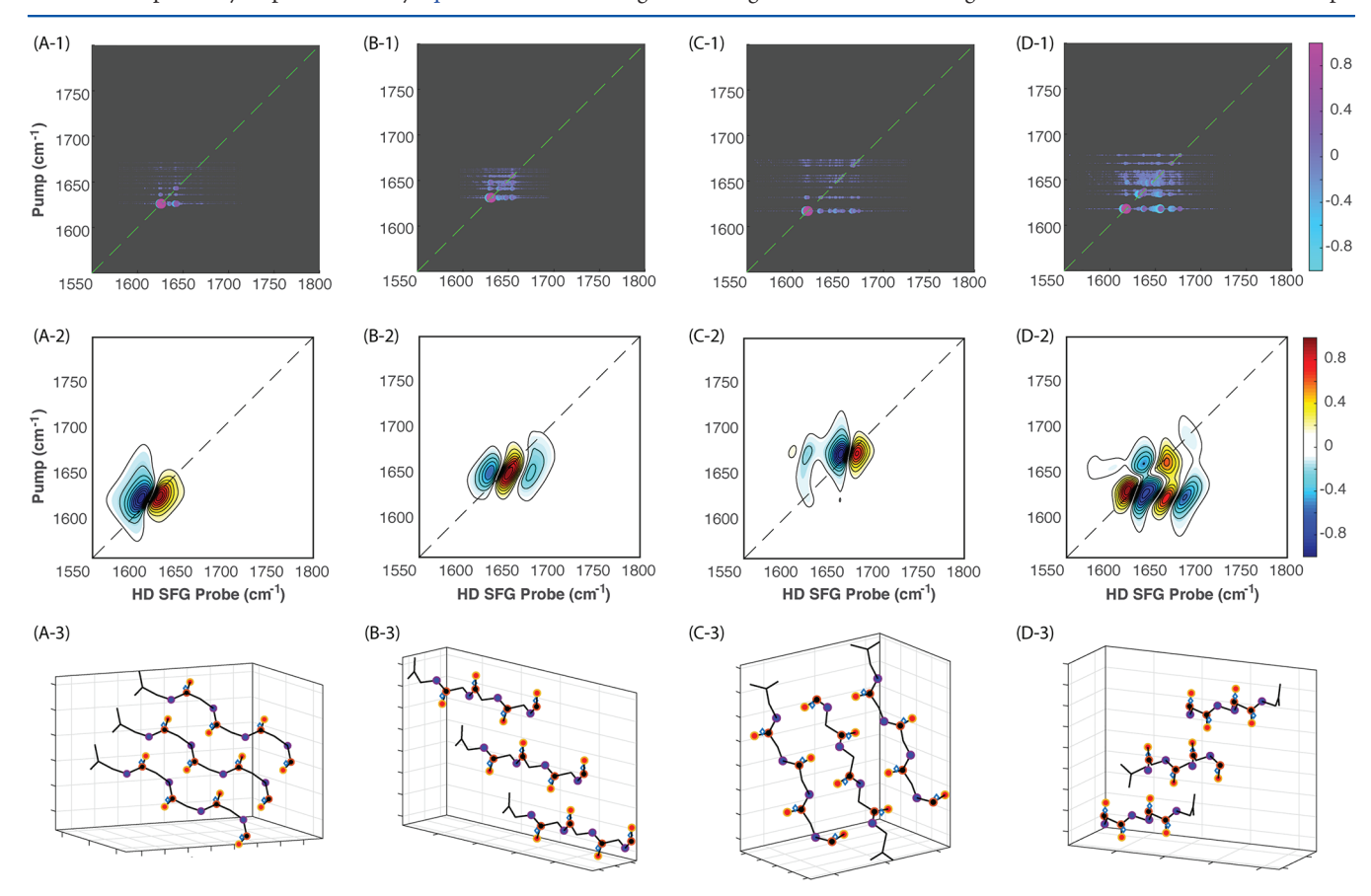


Figure 6. First row (A-1–D-1) shows the transition intensity spectrum, T, of the four β-sheet models. The second row (A-2–D-2) shows the simulated 2D SFG spectrum of the given orientations in the third row (A-3–D-3).

Without altering the interactions between molecules, a change of the molecular orientation results in a rotation (\hat{R}) of the molecular response $(\vec{\beta}^{(4)})$. The action of the rotation in the tensor notation can be moved out of the molecular response:

$$S(\phi, \psi, \theta) \propto \hat{R}(\phi, \psi, \theta) \cdot \vec{\beta}^{(4)}$$
 (2)

This separation is important because $\vec{\beta}^{(4)}$ can be calculated at a fixed orientation and thus needs not to be repeatedly calculated. The rotational tensor \hat{R} has an analytical form so the calculation is significantly faster. Thus, we calculate all the Feynman paths in the molecular response once and then multiply this response by the rotational tensor for a given Euler angles. For 100

different orientations of a 15 residues polypeptide, the calculation is 100-fold more efficient per structure investigated.

One useful outcome of this mathematical formula is that we can quickly make plots that graphically illustrate the peak intensities as a function of molecular rientation. Shown in Figure 5 A is a 2D transition strengths (T) calculated from the molecular response $(\vec{\beta}^{(4)})$. We define the transition strength, T, as

$$T = \pm |\vec{\beta}_{ijklm}^{(4)}| = \pm |\vec{\alpha}_{ij}| \cdot |\vec{\mu}_{k}| \cdot |\vec{\mu}_{l}| \cdot |\vec{\mu}_{m}| \tag{3}$$

so that the transition strength gives the relative weights of each Feynman path (and their sign), but T is itself independent of orientation (see Supporting Information for more information). The plot is used to visualize the locations of diagonal and cross

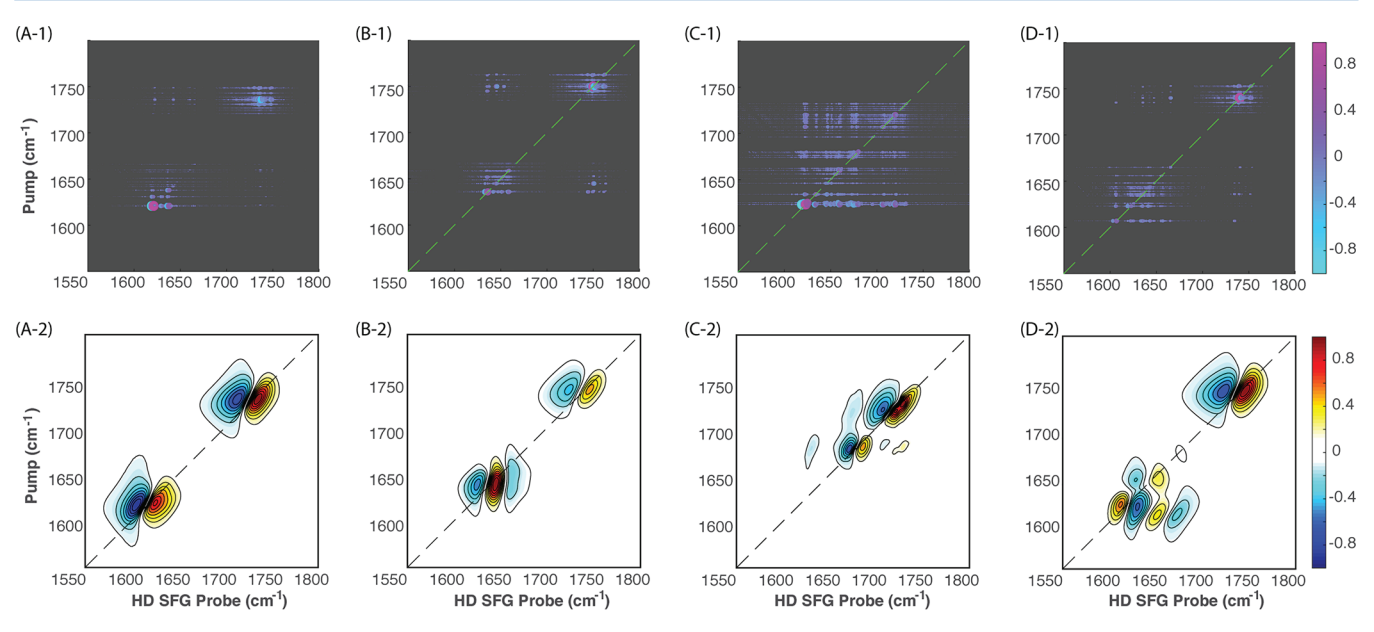


Figure 7. First row (A-1-D-1) shows the transition intensity spectrum of the four β-sheet on the MBA monolayer. The second row is the 2D SFG spectrum of four structural models described in the text.

peaks, from which we choose peaks or integrate regions of peaks that we want to optimize for comparison to experiment. Those peaks or regions are then calculated using eq 1 as a function of Euler angles and graphically plotted as 3D contour plots. For example, we show a 2D transition strength spectrum for an ideal β -sheet (Figure 5A), along with the orientational dependence for the diagonal (Figure 5B) and cross peak (Figure 5C) regions enclosed in colored squares. The orientational dependency of the diagonal peak are very different from the cross peak because the diagonal peaks only depend on the transition dipoles and the polarizabilities for a single vibrational mode whereas the cross peaks depend on two vibrational modes. These plots are then used to find orientations that are consistent with the intensities and signs measured in the experiment. For the final comparison, we convolute with a homogeneous line shape and add diagonal disorder, as described in the Materials and Methods section.

Simulations of Parallel and Antiparallel β -Sheet Structures. The diagonal peak at 1620 cm⁻¹ in both Figures 2 and 3 is strong evidence for β -sheet formation. With that experimental assignment in mind, we start with a β -strand with four peptide bonds created by five residues of the FGAIL sequence. We perform the simulations using three strands because we find that the transition strengths of the dominant modes are about constant for β -sheets larger than 3 strands (both parallel and antiparallel) and additional frequency shifts are small (Supporting Information).

Shown in Figure 6 are 2D SFG spectra calculated from four different β -sheet structures. Two structures are of parallel (A, B) and the other two are antiparallel (C, D) β -sheet. Of these β -sheets, two are canonical structure (A, C) and two have off-register structures (B, D) in which residue n in one β -sheet is hydrogen bonded to residue n+1 in the adjacent strand. Off-register structures are found in many amyloid and tubular structures created from self-assembled peptides. For each of these β -sheets, the signal orientation dependency maps were calculated and shown in the Supporting Information (Figure S4). The choice of orientation alters the relative signal intensities (S) of the peaks in the 2D SFG spectra, depending

on how well-aligned the transition dipoles and polarizability tensors are to the incident laser pulse polarizations.

Similar to a typical β -sheet 2D IR, the 2D SFG of the canonical parallel β -sheet (Figure 6A-3) shows a strong transition near 1620 cm⁻¹ (Figure 6A-1) with an anharmonically shifted overtone peak (Figure 6A-2). Because both the transition dipole and polarizability strengths of this mode are much larger than others, the 2D SFG spectrum is dominated by the 1620 cm⁻¹ transition unless the β -sheets oriented in a narrow range of angles ($\theta \approx 90^{\circ}$) that put this mode orthogonal to the surface. We also tried to simulate both peaks F and H in Figure 2 using the canonical β -sheet (Figure 6A-3) structure and found that a concomitant positive cross peak appears close to the cross peak GD (Figure SS), which does not match the experimental spectrum. An off-register structure produces a similar spectrum but with a much more prominent transition strength (T) around 1650 cm⁻¹ (Figure 6B-1).

An antiparallel β -sheet can also exhibit a strong 1620 cm⁻¹ band (Figure 6 C-1), but unlike parallel sheets, antiparallel sheets also have modes above 1650 cm⁻¹. At some orientations (Figure 6 C-3), the high-frequency mode can dominate (Figure 6 C-2), which appears at \approx 1670 cm⁻¹. Off-register antiparallel β -sheets are interesting because they have significant cross peaks transition strength (T) that can appear very strong on the lower half of the diagonal (Figure 6D-2), creating by couplings between the 1620 and 1670 cm⁻¹ modes.

Peptide Monolayer Coupling. In this section, we investigate the origin of the cross peaks between the MBA and FGAIL features, labeled AE, CE, and CA in Figure 2. For each of the four structures simulated in Figure 6, we now add the 4-by-4 MBA monolayer model (Figure 4, AP). We place the FGAIL peptide about one hydrogen-bond length above (\approx 2 Å) the MBA headgroups. The resulting spectra are shown in Figure 7. The fundamental frequencies of the protein and MBA peaks are not altered significantly because of the large frequency difference between the MBA and FGAIL local modes. However, the peak intensities are more sensitive to couplings

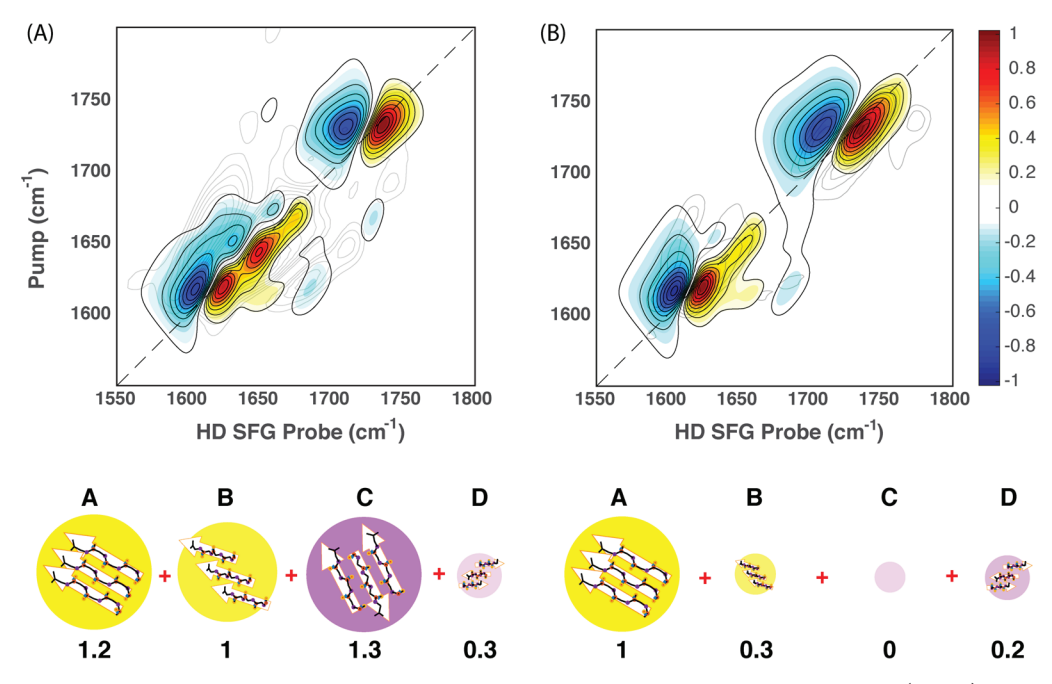


Figure 8. Simulated 2D SFG spectrum generated by summing four β-sheet models from Figures 7. Yellow (purple) circles enclose parallel (antiparallel) β-sheet. The circle size and transparency reflect the structure mixing ratio. (A) FGAIL on MBA monolayer using relative weights A:B:C:D = 1.2:1:1.3:0.3 where labels A to D refer to the structure presented in the Figure 6A-3–D-3. (B) FGAIL tethered to MBA using relative weights A:B:C:D = 1:0.3:0:0.2. The gray contour lines are the corresponding experimental spectra for visual reference from Figures 2 and 3, respectively.

than are frequencies.⁶⁹ In these simulations, we find the maximum coupling strength is $\approx 20 \text{ cm}^{-1}$.

Of these four simulations, we see cross peaks analogous to CA, for MBA with the antiparallel in-register structure (Figure 7C). That structure (Figure 6C-3) best matches experiment, with the cross peak appearing at about 1675 cm⁻¹ (Figure 7C-2). The dominating peptide vibrations of the other three structures have frequencies that are more remote from the MBA vibrational frequencies, creating much weaker cross peaks that are not resolved with these contour levels. If they are present in the experiments, higher signal-to-noise would be required to resolve them.

Heterogeneous Populations of β -Sheet Structures Describe Experiment. From these simulations, we conclude that the 2D SFG spectrum cannot be described by a single aggregate structure. None of our simulations were able to simultaneously create peaks E, F, and H all with similar intensities and phases. We were able to generate structures with two prominent modes, such as the parallel canonical β -sheet, as well as antiparallel sheets (see Supporting Information Figure S4), but never in the correct ratios with the proper spread of frequencies and matching cross peaks. Taking into account the experimental evidence that covalently linking the peptides to the surfaces alters the intensities of the peaks without dramatic changes in frequency, we conclude that the spectra are best described by a distribution of polypeptide structures.

Having made this assessment, we used weighted sums of the spectra in Figure 7 to simulate a spectrum that best describes the experiments within our modeling, shown in Figure 8 (the experimental data is shown gray for reference). Better agreement with experiment might occur by simulating an ensemble of more diverse structure, suggesting that physisorption induces a very high degree of heterogeneity. As of now, we focused on reproducing the strongest defining features of the experiments, which are the three positive diagonal peaks

E, F, and H; the peptide cross peaks GD and FB; and the FGAIL-MBA cross peaks AE and CA. Shown in Figure 8A is a summation of the 2D SFG spectra from Figure 7A-2–D-2, weighted via relative ratios of 1.2:1:1.3:0.3, respectively. These spectra correspond to the parallel in-register, parallel off-register, antiparallel in-register, and antiparallel off-register β -sheets, respectively. Many different combinations of structures can be used to generate the three diagonal peaks, but only the antiparallel in-register β -sheet structure created the cross peaks AE and CA to the MBA headgroups at close to the proper frequencies. Similarly, an antiparallel off-register structure was needed to generate the FGAIL cross peak GD (our simulations did not reproduce cross peak FB).

Shown in Figure 8B is a simulation using the same four subensemble structures, but adding in the relative ratios 1:0.3:0:0.2. In this simulation, most of the ensemble weight is given to the parallel β -sheet structure with the tilted FGAIL strands sticking up to the MBA surface (Figure 6A-3). This simulation is similar to the 2D SFG spectrum for covalently linked FGAIL-MBA monolayers (Figure 3); the 1620 cm⁻¹ peak is the strongest, with very little cross peak intensity. Indeed, the covalently linked FGAIL peptides might be expected to be parallel because they are oriented by the linkage. When serving as nucleation points or seeds to additional peptides from solution or other peptides linked to the monolayer, these strands primarily favor parallel sheet or other protein aggregate structures.

Thus, we find that an ensemble of structures is able to qualitatively describe both experimental 2D SFG spectra, albeit with different subensemble populations. The population skews to parallel sheets for FGAIL peptides that are covalently link to the monolayer, and thereby provide directional constraints to aggregation. Thus, a broad distribution of protein structures is indicative of a nonselective aggregation or heterogeneous set of

aggregation mechanisms whereas a narrow distribution implies a structurally directed self-assembly process.

DISCUSSION

Biological membranes typically catalyze the formation of amyloid aggregates. ^{29,71,72} In solution, model membrane vesicles can speed up amyloid fibril formation 10-fold, often losing the characteristic sigmoidal kinetic curve, but instead exhibiting exponential growth.⁷³ Whether this process is important for the disease mechanism is up for debate, because nonbiological surfaces like nanoparticles also speed aggregation. 4 Because amyloid fiber formation is thought to be a nucleation and growth mechanism, surfaces might simply increase local concentrations and thereby the likelihood for nucleation. Alternatively, surfaces might favor one aggregation mechanism over another, such as by stabilizing an intermediate. In solution, uncontrolled aggregation conditions often lead to a distribution of polymorphic structures, whereas aggregation under very controlled conditions is often necessary to form proteins with a single polymorph.⁷⁵ Thus, a distribution of polymorph structure would be consistent with a nonselective process whereas a well-defined fiber structure would imply a directed or favored aggregation pathway.

Our experiments find that FGAIL adopts a distribution of parallel and antiparallel β -sheet structures on the hydrogen bonding monolayer made from MBA. Thus, MBA itself does not strongly direct the aggregation process. The results are more consistent with aggregation occurring at an effectively higher concentration that creates low entropy-driven nucleation barriers leading to a broader range of polymorphs. In other words, the MBA surface promotes many nucleation structures creating fiber aggregates with many structures, such as schematically shown in Figure 9A. In contrast, our experiments

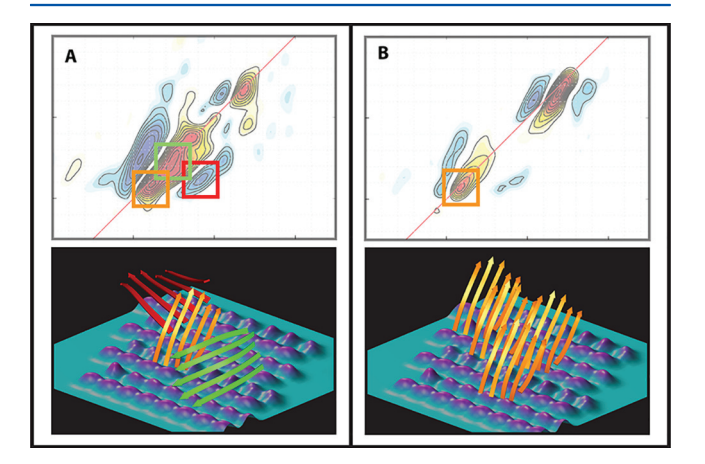


Figure 9. Selected 2D SFG features with their corresponding cartoon schematics in system (A) FGAIL on MBA monolayer (B) FGAIL tethered on the MBA monolayer.

find that if the surface is prepared with oriented FGAIL polypeptides, then primarily one aggregate structure and orientation is preferred over the others (Figure 9B). Thus, the effects created by a 2D surface concentrating the peptides can be counterbalanced by membrane components that favor directed fiber growth. In more realistic membranes, directed growth might be caused by specific lipid components, like gangliosides, 28 membrane proteins, 17 or the stabilization of intermediates like α -helices. 16,30

FGAIL serves as a model for possible outcomes of membrane-catalyzed amyloid formation. FGAIL is a fragment of the full length hIAPP polypeptide. The full length protein consists of 37 amino acids and so presumably has a lower free energy minimum for a preferred structure or a preferred orientation on a membrane. Nonetheless, it is known that the FGAIL region of the full length hIAPP protein is a critical region for aggregation. Single-site mutations in this region can dramatically alter fibril morphology, according to TEM. In simulations, short polypeptides involving the FGAIL region are known to form both in-register and off-register polymorphs. Thus, our experiments are consistent with simulations that predict both parallel and antiparallel polymorphs for FGAIL that could be a factor in selecting the fibril polymorphs for full length hIAPP.

Though the data are reasonably described by the four structures presented here, there could be additional protein structures that are also consistent with our data. In principle, it is possible to extract orientational distributions from standard SFG spectra. 81-83 Variations of these procedures might be developed for 2D SFG spectroscopy. We are also assuming that the monolayer is undisrupted by FGAIL, but the MBA monolayer might be reorganizing to accommodate the backbone or side chains. Indeed, the amide-I modes that are probed in our experiments do not give information on side chain conformations. 2D SFG spectroscopy can be rigorously simulated from molecular dynamics simulations.⁸⁴ Thus, much more realistic protein and membrane protein structures might be generated from atomistic molecular dynamics simulations from which the 2D SFG data are simulated for comparison to experiment, as has been done for nonchiral and chiral SFG experiments as well as 2D IR experiments on membrane proteins.85-87

Besides 2D SFG spectroscopy, it has recently become possible to measure monolayers with 2D IR spectroscopy, which also provides coupling information through cross peaks. ^{53,88,89} Although surface-sensitive 2D IR spectroscopy has not yet been applied to proteins, it is clear that the additional information provided by cross peaks in 2D IR and 2D SFG spectroscopy is extremely valuable for ascertaining distributions of structures. In surface-specific 2D IR spectroscopy, the kinetic exchange between monolayers has now been identified through the kinetics of cross peaks. ⁹⁰ These new generations of surface-specific multidimensional spectroscopies promise to open up many new avenues of research in biological and nonbiological surface science.

CONCLUSION

In conclusion, we have shown, via heterodyne-detected 2D SFG spectroscopy, that FGAIL peptides spontaneously form mixtures of parallel and antiparallel β -sheets on a hydrogen bond promoting surface made from the carboxylic acids headgroup of MBA self-assembled monolayer. The 2D SFG spectra could not be simulated from a single protein conformation, but a weighted sum of four different conformations were used to recreate the spectrum. A single protein conformation was found when FGAIL peptides were covalently linked to the monolayer, thereby directing the growth of aggregates. These experiments extend 2D SFG spectroscopy to β -sheets, helping to develop their spectroscopic signatures. The results suggest that surfaces with hydrogen bonding properties, like those present in natural bilayers, may

help explain the presence of polymorphs of amyloid fibers that are known to exist in disease-associated proteins.

ASSOCIATED CONTENT

Supporting Information

The Supporting Information is available free of charge on the ACS Publications website at DOI: 10.1021/acs.jpca.7b11934..

DFT calculation details, 2D SFG (MMB) monolayer on gold, definition of transition strengths for IR and Raman processes, transition strength dependency of peptide models, and orientation analysis of the peptide models (PDF)

AUTHOR INFORMATION

Corresponding Author

*M. T. Zanni. E-mail: zanni@chem.wisc.edu.

ORCID ©

Jia-Jung Ho: 0000-0002-9767-8082 Ayanjeet Ghosh: 0000-0001-9458-3910 Martin T. Zanni: 0000-0001-7191-9768

Notes

The authors declare the following competing financial interest(s): To avoid conflicts of interest, M.T.Z. is obligated to disclose that he is an owner of PhaseTech Spectroscopy, Inc., which sells pulse shapers and 2D spectrometers.

ACKNOWLEDGMENTS

The authors thank the NSF for funding the instrument and methodology development through grant CHE-1665110 and the NIH for the peptide work through grant DK079895. The authors also thank Dr. Arnaldo Serrano for constructive discussions.

■ REFERENCES

- (1) Love, J. C.; Estroff, L. A.; Kriebel, J. K.; Nuzzo, R. G.; Whitesides, G. M. Self-Assembled Monolayers of Thiolates on Metals as a Form of Nanotechnology. *Chem. Rev.* **2005**, *105*, 1103–1170.
- (2) Li, S.; Mehta, A. K.; Sidorov, A. N.; Orlando, T. M.; Jiang, Z.; Anthony, N. R.; Lynn, D. G. Design of Asymmetric Peptide Bilayer Membranes. J. Am. Chem. Soc. 2016, 138 (10), 3579–3586.
- (3) Coppage, R.; Slocik, J. M.; Briggs, B. D.; Frenkel, A. I.; Heinz, H.; Naik, R. R.; Knecht, M. R. Crystallographic Recognition Controls Peptide Binding for Bio-Based Nanomaterials. *J. Am. Chem. Soc.* **2011**, 133 (32), 12346–12349.
- (4) Cao, P.; Marek, P.; Noor, H.; Patsalo, V.; Tu, L.-H.; Wang, H.; Abedini, A.; Raleigh, D. P. Islet Amyloid: From Fundamental Biophysics to Mechanisms of Cytotoxicity. *FEBS Lett.* **2013**, *587* (8), 1106–1118.
- (5) Stroud, J. C.; Liu, C.; Teng, P. K.; Eisenberg, D. Toxic Fibrillar Oligomers of Amyloid- Have Cross- Structure. *Proc. Natl. Acad. Sci. U. S. A.* **2012**, *109* (20), 7717–7722.
- (6) Khemtémourian, L.; Antoinette Killian, J.; Höppener, J. W. M.; Engel, M. F. M. Recent Insights in Islet Amyloid Polypeptide-Induced Membrane Disruption and Its Role in β -Cell Death in Type 2 Diabetes Mellitus. *Exp. Diabetes Res.* **2008**, 2008, 1–9.
- (7) Buchanan, L. E.; Dunkelberger, E. B.; Tran, H. Q.; Cheng, P.-N.; Chiu, C.-C.; Cao, P.; Raleigh, D. P.; de Pablo, J. J.; Nowick, J. S.; Zanni, M. T. Mechanism of IAPP Amyloid Fibril Formation Involves an Intermediate with a Transient -Sheet. *Proc. Natl. Acad. Sci. U. S. A.* **2013**, *110* (48), 19285–19290.
- (8) Tycko, R. Solid-State NMR Studies of Amyloid Fibril Structure. *Annu. Rev. Phys. Chem.* **2011**, 62 (1), 279–299.

- (9) Kayed, R. Common Structure of Soluble Amyloid Oligomers Implies Common Mechanism of Pathogenesis. *Science* **2003**, *300* (5618), 486–489.
- (10) Vácha, R.; Linse, S.; Lund, M. Surface Effects on Aggregation Kinetics of Amyloidogenic Peptides. *J. Am. Chem. Soc.* **2014**, *136* (33), 11776–11782.
- (11) Qiao, Q.; Bowman, G. R.; Huang, X. Dynamics of an Intrinsically Disordered Protein Reveal Metastable Conformations That Potentially Seed Aggregation. *J. Am. Chem. Soc.* **2013**, *135* (43), 16092–16101.
- (12) Abelein, A.; Jarvet, J.; Barth, A.; Gräslund, A.; Danielsson, J. Ionic Strength Modulation of the Free Energy Landscape of $A\beta$ 40 Peptide Fibril Formation. *J. Am. Chem. Soc.* **2016**, *138* (21), 6893–6902.
- (13) Wärmländer, S.; Tiiman, A.; Abelein, A.; Luo, J.; Jarvet, J.; Söderberg, K. L.; Danielsson, J.; Gräslund, A. Biophysical Studies of the Amyloid β -Peptide: Interactions with Metal Ions and Small Molecules. *ChemBioChem* **2013**, *14* (14), 1692–1704.
- (14) Shafrir, Y.; Durell, S.; Arispe, N.; Guy, H. R. Models of Membrane-Bound Alzheimer's Abeta Peptide Assemblies. *Proteins: Struct., Funct., Genet.* **2010**, 78 (16), 3473–3487.
- (15) Whitesides, G. M.; Mathias, J. P.; Seto, C. T. Molecular Self-Assembly and Nanochemistry: A Chemical Strategy for the Synthesis of Nanostructures. *Science* **1991**, *254* (5036), 1312–1319.
- (16) Fu, L.; Liu, J.; Yan, E. C. Y. Chiral Sum Frequency Generation Spectroscopy for Characterizing Protein Secondary Structures at Interfaces. *J. Am. Chem. Soc.* **2011**, *133* (21), 8094–8097.
- (17) Zhang, M.; Ren, B.; Liu, Y.; Liang, G.; Sun, Y.; Xu, L.; Zheng, J. Membrane Interactions of HIAPP Monomer and Oligomer with Lipid Membranes by Molecular Dynamics Simulations. *ACS Chem. Neurosci.* **2017**, *8* (8), 1789–1800.
- (18) Lipids and Cellular Membranes in Amyloid Diseases; Jelinek, R., Ed.; Wiley-VCH: Weinheim, 2011.
- (19) Kazlauskaite, J.; Sanghera, N.; Sylvester, I.; Vénien-Bryan, C.; Pinheiro, T. J. T. Structural Changes of the Prion Protein in Lipid Membranes Leading to Aggregation and Fibrillization †. *Biochemistry* **2003**, 42 (11), 3295–3304.
- (20) Chirita, C. N.; Necula, M.; Kuret, J. Anionic Micelles and Vesicles Induce Tau Fibrillization in Vitro. *J. Biol. Chem.* **2003**, 278 (28), 25644–25650.
- (21) Jayasinghe, S. A.; Langen, R. Membrane Interaction of Islet Amyloid Polypeptide. *Biochim. Biophys. Acta, Biomembr.* **2007**, *1768* (8), 2002–2009.
- (22) Lorenzo, A.; Razzaboni, B.; Weir, G. C.; Yankner, B. A. Pancreatic Islet Cell Toxicity of Amylin Associated with Type-2 Diabetes Mellitus. *Nature* **1994**, *368* (6473), 756–760.
- (23) Cooper, G. J.; Leighton, B.; Dimitriadis, G. D.; Parry-Billings, M.; Kowalchuk, J. M.; Howland, K.; Rothbard, J. B.; Willis, A. C.; Reid, K. B. Amylin Found in Amyloid Deposits in Human Type 2 Diabetes Mellitus May Be a Hormone That Regulates Glycogen Metabolism in Skeletal Muscle. *Proc. Natl. Acad. Sci. U. S. A.* 1988, 85 (20), 7763–7766
- (24) Laganowsky, A.; Liu, C.; Sawaya, M. R.; Whitelegge, J. P.; Park, J.; Zhao, M.; Pensalfini, A.; Soriaga, A. B.; Landau, M.; Teng, P. K.; et al. Atomic View of a Toxic Amyloid Small Oligomer. *Science* **2012**, 335 (6073), 1228–1231.
- (25) Luca, S.; Yau, W.-M.; Leapman, R.; Tycko, R. Peptide Conformation and Supramolecular Organization in Amylin Fibrils: Constraints from Solid-State NMR †. *Biochemistry* **2007**, *46* (47), 13505–13522.
- (26) Cao, P.; Abedini, A.; Wang, H.; Tu, L.-H.; Zhang, X.; Schmidt, A. M.; Raleigh, D. P. Islet Amyloid Polypeptide Toxicity and Membrane Interactions. *Proc. Natl. Acad. Sci. U. S. A.* **2013**, *110* (48), 19279–19284.
- (27) Pilkington, E. H.; Gurzov, E. N.; Kakinen, A.; Litwak, S. A.; Stanley, W. J.; Davis, T. P.; Ke, P. C. Pancreatic β -Cell Membrane Fluidity and Toxicity Induced by Human Islet Amyloid Polypeptide Species. *Sci. Rep.* **2016**, *6* (1), 21274.

- (28) Wakabayashi, M.; Matsuzaki, K. Ganglioside-Induced Amyloid Formation by Human Islet Amyloid Polypeptide in Lipid Rafts. *FEBS Lett.* **2009**, 583 (17), 2854–2858.
- (29) Jayasinghe, S. A.; Langen, R. Lipid Membranes Modulate the Structure of Islet Amyloid Polypeptide †. *Biochemistry* **2005**, *44* (36), 12113–12119.
- (30) Maj, M.; Lomont, J. P.; Rich, K. L.; Alperstein, A. M.; Zanni, M. T. Site-Specific Detection of Protein Secondary Structure Using 2D IR Dihedral Indexing: A Proposed Assembly Mechanism of Oligomeric HIAPP. *Chem. Sci.* **2018**, *9*, 463.
- (31) Griffiths, J. M.; Ashburn, T. T.; Auger, M.; Costa, P. R.; Griffin, R. G.; Lansbury, P. T. Rotational Resonance Solid-State NMR Elucidates a Structural Model of Pancreatic Amyloid. *J. Am. Chem. Soc.* 1995, 117 (12), 3539–3546.
- (32) Middleton, C. T.; Marek, P.; Cao, P.; Chiu, C.; Singh, S.; Woys, A. M.; de Pablo, J. J.; Raleigh, D. P.; Zanni, M. T. Two-Dimensional Infrared Spectroscopy Reveals the Complex Behaviour of an Amyloid Fibril Inhibitor. *Nat. Chem.* **2012**, *4* (5), 355–360.
- (33) Prime, K.; Whitesides, G. Self-Assembled Organic Monolayers: Model Systems for Studying Adsorption of Proteins at Surfaces. *Science* **1991**, 252 (5009), 1164–1167.
- (34) McMasters, M. J.; Hammer, R. P.; McCarley, R. L. Surface-Induced Aggregation of Beta Amyloid Peptide by ω-Substituted Alkanethiol Monolayers Supported on Gold. *Langmuir* **2005**, *21* (10), 4464–4470.
- (35) Wang, Q.; Zhao, C.; Zhao, J.; Wang, J.; Yang, J.-C.; Yu, X.; Zheng, J. Comparative Molecular Dynamics Study of $A\beta$ Adsorption on the Self-Assembled Monolayers. *Langmuir* **2010**, 26 (5), 3308–3316.
- (36) Kovalchuk, M. V.; Kazimirov, A. Y.; Zheludeva, S. I. Surface-Sensitive X-Ray Diffraction Methods: Physics, Applications and Related X-Ray and SR Instrumentation. *Nucl. Instrum. Methods Phys. Res., Sect. B* **1995**, *101* (4), 435–452.
- (37) Krimm, S.; Bandekar, J. Vibrational Spectroscopy and Conformation of Peptides, Polypeptides, and Proteins. In *Advances in Protein Chemistry*; Anfinsen, C. B., Edsall, J. T., Richards, F. M., Eds.; Academic Press, 1986; Vol. 38, pp 181–364.
- (38) Ding, B.; Panahi, A.; Ho, J.-J.; Laaser, J. E.; Brooks, C. L.; Zanni, M. T.; Chen, Z. Probing Site-Specific Structural Information of Peptides at Model Membrane Interface In Situ. *J. Am. Chem. Soc.* **2015**, 137 (32), 10190–10198.
- (39) Fu, L.; Xiao, D.; Wang, Z.; Batista, V. S.; Yan, E. C. Y. Chiral Sum Frequency Generation for In Situ Probing Proton Exchange in Antiparallel β -Sheets at Interfaces. *J. Am. Chem. Soc.* **2013**, *135* (9), 3592–3598.
- (40) Xiao, D.; Fu, L.; Liu, J.; Batista, V. S.; Yan, E. C. Y. Amphiphilic Adsorption of Human Islet Amyloid Polypeptide Aggregates to Lipid/Aqueous Interfaces. *J. Mol. Biol.* **2012**, 421 (4–5), 537–547.
- (41) Tatulian, S. A. Structural Characterization of Membrane Proteins and Peptides by FTIR and ATR-FTIR Spectroscopy. In *Lipid-Protein Interactions; Methods in Molecular Biology*; Humana Press: Totowa, NJ, 2013; pp 177–218.
- (42) Rabe, M.; Schwieger, C.; Zope, H. R.; Versluis, F.; Kros, A. Membrane Interactions of Fusogenic Coiled-Coil Peptides: Implications for Lipopeptide Mediated Vesicle Fusion. *Langmuir* **2014**, *30* (26), 7724–7735.
- (43) Shim, S.-H.; Gupta, R.; Ling, Y. L.; Strasfeld, D. B.; Raleigh, D. P.; Zanni, M. T. Two-Dimensional IR Spectroscopy and Isotope Labeling Defines the Pathway of Amyloid Formation with Residue-Specific Resolution. *Proc. Natl. Acad. Sci. U. S. A.* **2009**, *106* (16), 6614–6619.
- (44) Kolano, C.; Helbing, J.; Kozinski, M.; Sander, W.; Hamm, P. Watching Hydrogen-Bond Dynamics in a β -Turn by Transient Two-Dimensional Infrared Spectroscopy. *Nature* **2006**, 444, 469.
- (45) Lessing, J.; Roy, S.; Reppert, M.; Baer, M.; Marx, D.; Jansen, T. L. C.; Knoester, J.; Tokmakoff, A. Identifying Residual Structure in Intrinsically Disordered Systems: A 2D IR Spectroscopic Study of the GVGXPGVG Peptide. J. Am. Chem. Soc. 2012, 134 (11), 5032–5035.

- (46) Remorino, A.; Hochstrasser, R. M. Three-Dimensional Structures by Two-Dimensional Vibrational Spectroscopy. *Acc. Chem. Res.* **2012**, *45* (11), 1896–1905.
- (47) Hamm, P.; Zanni, M. T. Concepts and Methods of 2d Infrared Spectroscopy; Cambridge University Pres: Cambridge, U.K.; New York, 2011.
- (48) Shim, S.-H.; Strasfeld, D. B.; Ling, Y. L.; Zanni, M. T. Automated 2D IR Spectroscopy Using a Mid-IR Pulse Shaper and Application of This Technology to the Human Islet Amyloid Polypeptide. *Proc. Natl. Acad. Sci. U. S. A.* **2007**, *104* (36), 14197–14202.
- (49) Xiong, W.; Laaser, J. E.; Mehlenbacher, R. D.; Zanni, M. T. Adding a Dimension to the Infrared Spectra of Interfaces Using Heterodyne Detected 2D Sum-Frequency Generation (HD 2D SFG) Spectroscopy. *Proc. Natl. Acad. Sci. U. S. A.* **2011**, *108* (52), 20902–20907.
- (50) Singh, P. C. Ultrafast Vibrational Dynamics of Water at a Charged Interface Revealed by Two-Dimensional Heterodyne-Detected Vibrational Sum Frequency Generation. *J. Chem. Phys.* **2012**, *137* (9), 094706.
- (51) Hsieh, C.-S.; Okuno, M.; Hunger, J.; Backus, E. H. G.; Nagata, Y.; Bonn, M. Aqueous Heterogeneity at the Air/Water Interface Revealed by 2D-HD-SFG Spectroscopy. *Angew. Chem., Int. Ed.* **2014**, 53 (31), 8146–8149.
- (52) Li, Y.; Wang, J.; Clark, M. L.; Kubiak, C. P.; Xiong, W. Characterizing Interstate Vibrational Coherent Dynamics of Surface Adsorbed Catalysts by Fourth-Order 3D SFG Spectroscopy. *Chem. Phys. Lett.* **2016**, *650*, 1–6.
- (53) Kraack, J. P.; Hamm, P. Surface-Sensitive and Surface-Specific Ultrafast Two-Dimensional Vibrational Spectroscopy. *Chem. Rev.* **2017**, *117* (16), 10623–10664.
- (54) Urcuyo, R.; Cortés, E.; Rubert, A. A.; Benitez, G.; Montero, M. L.; Tognalli, N. G.; Fainstein, A.; Vela, M. E.; Salvarezza, R. C. Aromatic and Aliphatic Thiol Self-Assembled Monolayers on Au: Anchoring and Delivering Copper Species. *J. Phys. Chem. C* **2011**, *115* (50), 24707–24717.
- (55) Etayash, H.; Norman, L.; Thundat, T.; Stiles, M.; Kaur, K. Surface-Conjugated Antimicrobial Peptide Leucocin A Displays High Binding to Pathogenic Gram-Positive Bacteria. *ACS Appl. Mater. Interfaces* **2014**, 6 (2), 1131–1138.
- (56) Lombana, A.; Raja, Z.; Casale, S.; Pradier, C.-M.; Foulon, T.; Ladram, A.; Humblot, V. Temporin-SHa Peptides Grafted on Gold Surfaces Display Antibacterial Activity: ANTIMICROBIAL PEPTIDE: TEMPORINS ON GOLD SURFACES. *J. Pept. Sci.* **2014**, 20 (7), 563–569.
- (57) Ho, J.-J.; Skoff, D. R.; Ghosh, A.; Zanni, M. T. Structural Characterization of Single-Stranded DNA Monolayers Using Two-Dimensional Sum Frequency Generation Spectroscopy. *J. Phys. Chem. B* **2015**, *119* (33), 10586–10596.
- (58) Ghosh, A.; Ho, J.-J.; Serrano, A. L.; Skoff, D. R.; Zhang, T.; Zanni, M. T. Two-Dimensional Sum-Frequency Generation (2D SFG) Spectroscopy: Summary of Principles and Its Application to Amyloid Fiber Monolayers. *Faraday Discuss.* **2015**, *177*, 493–505.
- (59) Frisch, M. J.; Trucks, G. W.; Schlegel, H. B.; Scuseria, G. E.; Robb, M. A.; Cheeseman, J. R.; Scalmani, G.; Barone, V.; Petersson, G. A.; Nakatsuji, H.; et al. *Gaussian 09*; Gaussian, Inc.: Wallingford, CT, 2009.
- (60) la Cour Jansen, T.; Dijkstra, A. G.; Watson, T. M.; Hirst, J. D.; Knoester, J. Modeling the Amide I Bands of Small Peptides. *J. Chem. Phys.* **2006**, *125* (4), 044312.
- (61) Ho, J.-J. COSMOSS: Coupled Oscillator MOdel Spectrum Simulator. https://github.com/JJ-Ho/COSMOSS (accessed Nov 19, 2017).
- (62) Rosendahl, S. M.; Burgess, I. J. Electrochemical and Infrared Spectroscopy Studies of 4-Mercaptobenzoic Acid SAMs on Gold Surfaces. *Electrochim. Acta* **2008**, *53* (23), *6759–6767*.
- (63) Bakker, J. M.; Mac Aleese, L.; von Helden, G.; Meijer, G. The Infrared Absorption Spectrum of the Gas Phase Neutral Benzoic Acid Monomer and Dimer. *J. Chem. Phys.* **2003**, *119* (21), 11180–11185.

- (64) Karabacak, M.; Cinar, Z.; Kurt, M.; Sudha, S.; Sundaraganesan, N. FT-IR, FT-Raman, NMR and UV—vis Spectra, Vibrational Assignments and DFT Calculations of 4-Butyl Benzoic Acid. *Spectrochim. Acta, Part A* **2012**, *85* (1), 179—189.
- (65) Laaser, J. E.; Zanni, M. T. Extracting Structural Information from the Polarization Dependence of One- and Two-Dimensional Sum Frequency Generation Spectra. *J. Phys. Chem. A* **2013**, *117* (29), 5875–5890.
- (66) Pensa, E.; Rubert, A. A.; Benitez, G.; Carro, P.; Orive, A. G.; Creus, A. H.; Salvarezza, R. C.; Vericat, C. Are 4-Mercaptobenzoic Acid Self Assembled Monolayers on Au(111) a Suitable System to Test Adatom Models? *J. Phys. Chem. C* 2012, *116* (49), 25765–25771.
- (67) Simpson, G. J. Nonlinear Optical Polarization Analysis in Chemistry and Biology; Cambridge molecular science; Cambridge University Press: Cambridge, United Kingdom; New York, 2016.
- (68) Strodel, B.; Whittleston, C. S.; Wales, D. J. Thermodynamics and Kinetics of Aggregation for the GNNQQNY Peptide. *J. Am. Chem. Soc.* **2007**, *129* (51), 16005–16014.
- (69) Lomont, J. P.; Ostrander, J. S.; Ho, J.-J.; Petti, M. K.; Zanni, M. T. Not All β -Sheets Are the Same: Amyloid Infrared Spectra, Transition Dipole Strengths, and Couplings Investigated by 2D IR Spectroscopy. *J. Phys. Chem. B* **2017**, *121*, 8935.
- (70) Shaw, C. P.; Middleton, D. A.; Volk, M.; Lévy, R. Amyloid-Derived Peptide Forms Self-Assembled Monolayers on Gold Nanoparticle with a Curvature-Dependent β -Sheet Structure. *ACS Nano* **2012**, 6 (2), 1416–1426.
- (71) Knight, J. D.; Miranker, A. D. Phospholipid Catalysis of Diabetic Amyloid Assembly. *J. Mol. Biol.* **2004**, 341, 1175–1187.
- (72) Knight, J. D.; Hebda, J. A.; Miranker, A. D. Conserved and Cooperative Assembly of Membrane-Bound α -Helical States of Islet Amyloid Polypeptide†. *Biochemistry* **2006**, *45*, 9496–9508.
- (73) Liu, Y.; Peterson, D. A.; Schubert, D. Amyloid β Peptide Alters Intracellular Vesicle Trafficking and Cholesterol Homeostasis. *Proc. Natl. Acad. Sci. U. S. A.* **1998**, 95 (22), 13266–13271.
- (74) Wu, W.; Sun, X.; Yu, Y.; Hu, J.; Zhao, L.; Liu, Q.; Zhao, Y.; Li, Y. TiO2 Nanoparticles Promote β -Amyloid Fibrillation in Vitro. *Biochem. Biophys. Res. Commun.* **2008**, 373 (2), 315–318.
- (75) Tycko, R.; Wickner, R. B. Molecular Structures of Amyloid and Prion Fibrils: Consensus versus Controversy. *Acc. Chem. Res.* **2013**, *46* (7), 1487–1496.
- (76) Tu, L.-H.; Serrano, A. L.; Zanni, M. T.; Raleigh, D. P. Mutational Analysis of Preamyloid Intermediates: The Role of His-Tyr Interactions in Islet Amyloid Formation. *Biophys. J.* **2014**, *106* (7), 1520–1527.
- (77) Mo, Y.; Lu, Y.; Wei, G.; Derreumaux, P. Structural Diversity of the Soluble Trimers of the Human Amylin(20–29) Peptide Revealed by Molecular Dynamics Simulations. *J. Chem. Phys.* **2009**, *130* (12), 125101.
- (78) Colombo, G.; Daidone, I.; Gazit, E.; Amadei, A.; Di Nola, A. Molecular Dynamics Simulation of the Aggregation of the Core-Recognition Motif of the Islet Amyloid Polypeptide in Explicit Water. *Proteins: Struct., Funct., Genet.* **2005**, *59* (3), 519–527.
- (79) Zanuy, D.; Nussinov, R. The Sequence Dependence of Fiber Organization. A Comparative Molecular Dynamics Study of the Islet Amyloid Polypeptide Segments 22–27 and 22–29. *J. Mol. Biol.* **2003**, 329 (3), 565–584.
- (80) Melquiond, A.; Gelly, J.-C.; Mousseau, N.; Derreumaux, P. Probing Amyloid Fibril Formation of the NFGAIL Peptide by Computer Simulations. *J. Chem. Phys.* **2007**, *126* (6), 065101.
- (81) Guyot-Sionnest, P.; Hunt, J. H.; Shen, Y. R. Sum-Frequency Vibrational Spectroscopy of a Langmuir Film: Study of Molecular Orientation of a Two-Dimensional System. *Phys. Rev. Lett.* **1987**, *59* (14), 1597–1600.
- (82) Chen, H.; Gan, W.; Wu, B.; Wu, D.; Zhang, Z.; Wang, H. Determination of the Two Methyl Group Orientations at Vapor/Acetone Interface with Polarization Null Angle Method in SFG Vibrational Spectroscopy. *Chem. Phys. Lett.* **2005**, 408 (4), 284–289.
- (83) Wang, J.; Chen, C.; Buck, S. M.; Chen, Z. Molecular Chemical Structure on Poly(Methyl Methacrylate) (PMMA) Surface Studied by

- Sum Frequency Generation (SFG) Vibrational Spectroscopy. J. Phys. Chem. B 2001, 105 (48), 12118–12125.
- (84) Liang, C.; Jansen, T. L. C. Simulation of Two-Dimensional Sum-Frequency Generation Response Functions: Application to Amide I in Proteins. *J. Phys. Chem. B* **2013**, *117* (23), 6937–6945.
- (85) Poojari, C.; Xiao, D.; Batista, V. S.; Strodel, B. Membrane Permeation Induced by Aggregates of Human Islet Amyloid Polypeptides. *Biophys. J.* **2013**, *105* (10), 2323–2332.
- (86) Wang, Z.; Han, X.; He, N.; Chen, Z.; Brooks, C. L. Molecular Structures of C- and N-Terminus Cysteine Modified Cecropin P1 Chemically Immobilized onto Maleimide-Terminated Self-Assembled Monolayers Investigated by Molecular Dynamics Simulation. *J. Phys. Chem. B* **2014**, *118* (21), 5670–5680.
- (87) Kratochvil, H. T.; Carr, J. K.; Matulef, K.; Annen, A. W.; Li, H.; Maj, M.; Ostmeyer, J.; Serrano, A. L.; Raghuraman, H.; Moran, S. D.; et al. Instantaneous Ion Configurations in the K+ Ion Channel Selectivity Filter Revealed by 2D IR Spectroscopy. *Science* **2016**, 353 (6303), 1040–1044.
- (88) Oudenhoven, T. A.; Joo, Y.; Laaser, J. E.; Gopalan, P.; Zanni, M. T. Dye Aggregation Identified by Vibrational Coupling Using 2D IR Spectroscopy. *J. Chem. Phys.* **2015**, *142* (21), 212449.
- (89) Yan, C.; Yuan, R.; Pfalzgraff, W. C.; Nishida, J.; Wang, L.; Markland, T. E.; Fayer, M. D. Unraveling the Dynamics and Structure of Functionalized Self-Assembled Monolayers on Gold Using 2D IR Spectroscopy and MD Simulations. *Proc. Natl. Acad. Sci. U. S. A.* **2016**, 113 (18), 4929–4934.
- (90) Yan, C.; Thomaz, J. E.; Wang, Y.-L.; Nishida, J.; Yuan, R.; Breen, J. P.; Fayer, M. D. Ultrafast to Ultraslow Dynamics of a Langmuir Monolayer at the Air/Water Interface Observed with Reflection Enhanced 2D IR Spectroscopy. J. Am. Chem. Soc. 2017, 139, 16518.